Structural design of a double-layered porous hydrogel for effective mass transport

Hyejeong Kim, Hyeon Jeong Kim, Hyung Kyu Huh, Hyung Ju Hwang, and Sang Joon Lee

Articles you may be interested in

Rapid response of thermo-sensitive hydrogels with porous structures
Appl. Phys. Lett. **106**, 171909 (2015); 10.1063/1.4919585

A cell-laden nanofiber/hydrogel composite structure with tough-soft mechanical property
Appl. Phys. Lett. **102**, 211914 (2013); 10.1063/1.4808082

Designing tissue phantoms for ultrasonography and elastography with TiO 2 incorporated polyacrylamide hydrogels
AIP Conf. Proc. **1461**, 151 (2012); 10.1063/1.4736881

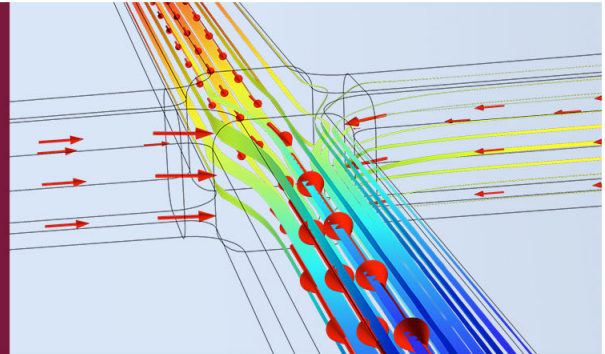Vascularization with trees that alternate with upside-down trees
J. Appl. Phys. **101**, 094904 (2007); 10.1063/1.2723186

Recent microgravity results in the synthesis of porous materials
AIP Conf. Proc. **458**, 88 (1999); 10.1063/1.57666

Structural design of a double-layered porous hydrogel for effective mass transport

Hyejeong Kim,[1] Hyeon Jeong Kim,[2] Hyung Kyu Huh,[1] Hyung Ju Hwang,[2] and Sang Joon Lee[1,a)]

[1]*Center for Biofluid and Biomimic Research and Department of Mechanical Engineering, Pohang University of Science and Technology, Pohang 790-784, South Korea*
[2]*Department of Mathematics, Pohang University of Science and Technology, Pohang 790-784, South Korea*

Mass transport in porous materials is universal in nature, and its worth attracts great attention in many engineering applications. Plant leaves, which work as natural hydraulic pumps for water uptake, have evolved to have the morphological structure for fast water transport to compensate large water loss by leaf transpiration. In this study, we tried to deduce the advantageous structural features of plant leaves for practical applications. Inspired by the tissue organization of the hydraulic pathways in plant leaves, analogous double-layered porous models were fabricated using agarose hydrogel. Solute transport through the hydrogel models with different thickness ratios of the two layers was experimentally observed. In addition, numerical simulation and theoretical analysis were carried out with varying porosity and thickness ratio to investigate the effect of structural factors on mass transport ability. A simple parametric study was also conducted to examine unveiled relations between structural factors. As a result, the porosity and thickness ratio of the two layers are found to govern the mass transport ability in double-layered porous materials. The hydrogel models with widely dispersed pores at a fixed porosity, i.e., close to a homogeneously porous structure, are mostly turned out to exhibit fast mass transport. The present results would provide a new framework for fundamental design of various porous structures for effective mass transport. © 2015 AIP Publishing LLC. [http://dx.doi.org/10.1063/1.4914383]

I. INTRODUCTION

Mass transport in porous media is abundant in many biological systems, and its usefulness attracts much attention for engineering applications such as drug delivery,[1,2] moisture-regulating fabric,[3–5] and wound dressings.[6–8] Many porous materials are heterogeneous made of different layers, and characterizing mass transport through the multi-layered porous media thus have been often studied due to its academic interest and practical applications. The capillary flow through multi-layered porous layers, such as packed beds of particles or absorbent materials, has been widely investigated experimentally and theoretically.[9–15] Reyssat *et al.*, studied the imbibition of a wetting fluid into layers of packed beads[13] and Shou *et al.*, studied the geometry induced asymmetric capillary flow to obtain the optimal geometry for fastest flow absorption.[10,11] However, little attention has been paid to the mass transport through multi-layered porous structure by chemical potential difference. Some authors have presented analytical solutions of solute transport in multi-layered porous media under various boundary or interface conditions.[16,17] Pontrelli and Monte employed a mathematical model to investigate the diffusion transport of a drug between two porous media.[18] However, they mainly focused to

---

a)Present address: 77, Cheongam-ro, Nam-gu, Pohang-si, Gyeongsangbuk-do 790-784, South Korea. Electronic mail: sjlee@postech.ac.kr. Fax: +82-54-279-3199.

9, 024104-1

identify the validity of analytical solutions with lack of experimental approaches. In addition, the effect of micro-scale structural factors of porous media on effective mass diffusion is not well understood.

Plant leaves are typical living nature with nano/micro porous structures, which have considerably evolved to have optimal structures as a survival strategy in extreme environmental stresses.[19] Inspired by functional advantageous features of plant leaves, some biomimetic technologies, such as evaporative micropumps and artificial leaves, have been developed.[20–24] Even though plants lose 95% of the water absorbed from the roots at the leaves by transpiration, they can successively cope with the water loss by fast water transport for survival.[25] Plant leaves are considered to have the double-layered porous structures, composed of tightly packed palisade mesophyll (PM) cell layer and loosely connected spongy mesophyll (SM) cell layer (Fig. 1(a)). The porous morphological structures of plant leaves exhibit considerable diversity among the species and their habitats (Fig. 1(b)).[25] The biodiversity of leaf internal structures raises questions about structural design for effective mass transport.

Inspired by the water transport pathways in plant leaves, a simple physical model of double layered porous structures was introduced in this study. Solute transport through hydrogel models with different internal structures was investigated experimentally and analytically. In the model system, solution is solely diffused through heterogeneous porous materials under the influence of chemical potential gradient. The transient mass diffusion by chemical potential difference through a porous material can be described by Fick's second law of diffusion, $\frac{\partial c}{\partial t} = D \frac{\partial^2 c}{\partial x^2}$, where c is the concentration, t is the time, D is the diffusion coefficient, and x is the direction of diffusion. Mass diffusion can be characterized by effective diffusion coefficient which is closely related with material structure. In this study, porosity and thickness ratio of the models are changed as structural factors to make several different types of models having different effective diffusion coefficients. This model study aims to investigate the effect of morphological design of porous media for effective mass transport. In addition, unveiled relations
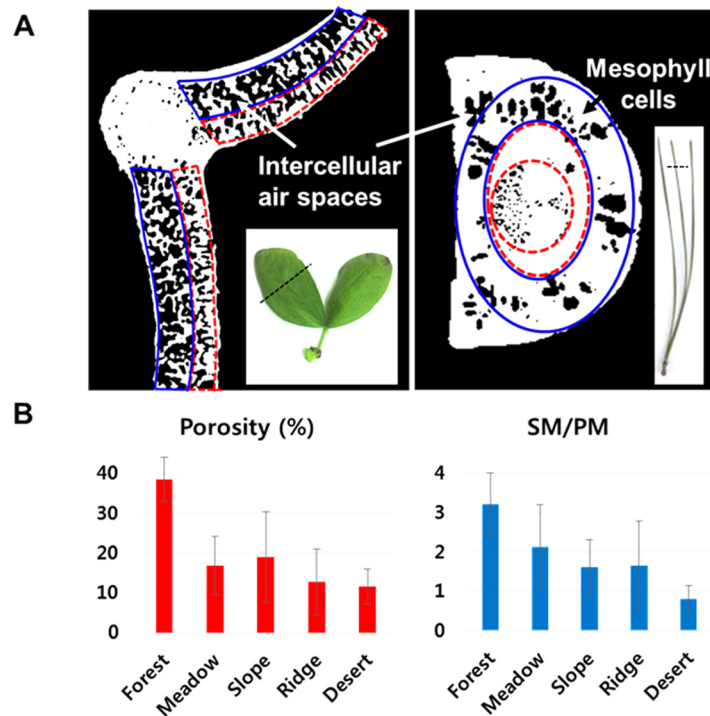

FIG. 1. (a) Cross-sectional images of *Vicia faba* (left) and pine needle (right). Black regions indicate intercellular air spaces and white regions denote mesophyll cells. Plant leaves consist of double-layered porous structures composed of PM (surrounded by solid line) and SM (surrounded by dashed line) cell layers. (b) Distributions of the porosity and thickness ratio (SM/PM) of 76 different species of real plant leaves depending on habitat.[25]

between structural factors were explored by using a parametric study. From these perspectives, this study is expected to provide a new framework for determining fundamental design parameters of porous structures for effective mass transport.

II. EXPERIMENTAL APPARATUS AND METHODS

A. Double-layered porous models

We investigated the transient diffusion of solution through double-layered porous media with a fixed average porosity and height. Three different kinds of porous structures in Figure 2 have identical average porosity, pore size, and total height. A porous medium with uniformly distributed pores through the structure (Fig. 2(a)) was used as the control sample to compare with other double-layer porous hydrogel models with different porosity gradients (Figs. 2(b) and 2(c)). The porous medium in Figure 2(a) has a height (L) and porosity (E), whereas each double layers in Figures 2(b) and 2(c) have two different porosities (ε_1) and (ε_2), with corresponding height (L_1) and (L_2), where $L_1 + L_2 = L$. We defined $\alpha(=L_2/L_1)$, which is the ratio of height between two layers. Thus, the relation of

$$\varepsilon_1 L_1 + \varepsilon_2 L_2 = LE \qquad (1)$$

is satisfied. Each configuration of double-layer structures is named as forward (Fig. 2(b), $\varepsilon_2 \sim 0$) when the more porous layer is placed at the bottom, and backward (Fig. 2(c), $\varepsilon_1 \sim 0$) when the less porous layer is placed at the bottom.

B. Double-layered porous agarose gel

Water-permeable agarose hydrogels were used as the primary material of the double-layered porous media. Agarose (Agarose-LE, Affymetrix, Inc., CA, USA) powder was suspended in water to obtain 2% concentration in solution. The suspension was heated until the agarose was fully dissolved. The viscosity of the agarose solution was measured with Brookfield viscometer, while dropping the temperature of the solution gradually from $49\,^\circ$C (at which agarose solution is in liquid) to $33\,^\circ$C around which gelation occurs (Fig. 3(a)). A leaching method was employed to make a double-layered porous agarose gel. Water-soluble isomalt particles, which were used as leaching particles, were sieved to obtain an average diameter of 750 μm. Agarose solution was poured into an acrylic container and isomalt particles were mixed in the solution. The terminal velocity of isomalt particles was determined (Fig. 3(b)) when all the forces applied to the isomalt particles reached an equilibrium condition (buoyancy force ($F_b = V_I \cdot \sigma \cdot g$) + viscous drag force ($F_d = 6\pi \cdot \eta \cdot v \cdot r$) = gravitational force ($F_g = V_I \cdot \rho \cdot g$), V_I: volume of isomalt particle, σ: density of solution (≈ 1 g/cm^3), g: acceleration of gravity , η: viscosity of solution, v: terminal velocity, and ρ: density of particle (=1.69 g/cm^3)). The Reynolds number of the system is
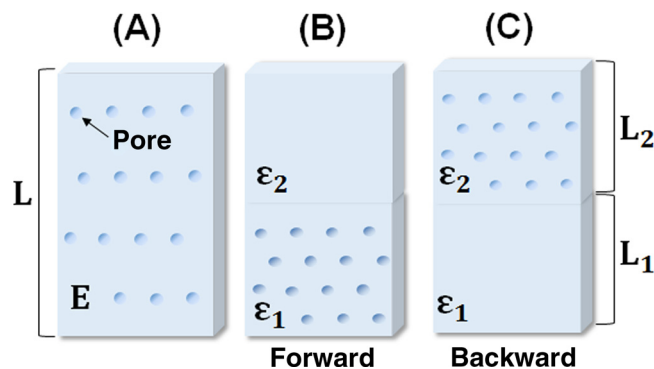

FIG. 2. Sketch of three different kinds of porous structures, whose average porosities, pore sizes, and total heights are identical. (a) A porous medium with uniformly distributed pores through the structure was used as the control sample. (b) and (c) Double-layer porous structures with porosity gradient.
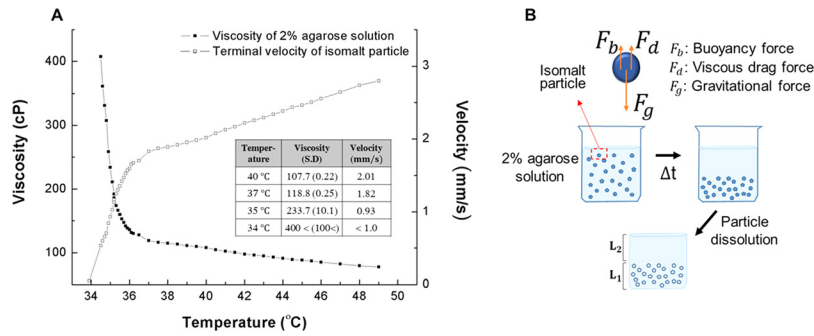
FIG. 3. Fabrication of double-layered porous agarose gel (a) Variation in viscosity of 2% agarose solution according to temperature, represented as filled dots. The variation in terminal velocity of isomalt particles inside the solution is represented as empty dots. (b) Sketch of the fabrication procedure of a double-layered porous structure.

very small (≤ 0.027). Therefore, in this study, the Stokes equation can be used to evaluate the drag force ($F_d = 6\pi \cdot \eta \cdot v \cdot r$). To make double-layered structures of which α is 0.5, 1, 2, and infinite (homogeneous), isomalt particles were inserted into solutions of 40, 37, 35, and 34 °C, respectively. At each temperature, viscosity of the solution was 107.7, 118.8, 233.7, and more than 400. The corresponding terminal velocity was 2.01, 1.82, 0.93, and less than 1.0 mm/s, respectively (Fig. 3(a)). The acrylic containers were dipped into ice water so that the falling isomalt particles stopped at proper locations to establish double-layered porous agarose gel models (Fig. 4(a_1–d_1)). The agarose gels were washed for 2 days with deionized water (DI) in the oven chamber at 70 °C to melt the isomalt particles. The double-layered structure was fabricated after dissolving out the isomalt particles with remaining voids (Fig. 3(b)).

C. 3D tomography of agarose models using synchrotron X-ray microscopy

3D morphological structures of the porous agarose gel models were observed by using X-ray micro-computed tomography at the 6C (bio-imaging) beamline at the Pohang Accelerator Laboratory (Pohang, Korea). Pieces of the porous gels were carefully cut and attached to a sample holder, which was then rotated from 0° to 180° at intervals of 0.5°. X-ray images were consecutively captured every 1 s at each angle of rotation. The X-ray images were converted into visible light by passing through a scintillator crystal and captured with a CCD camera of 2560×2160 pixel resolution (Andor Zyla). A 4× objective lens was attached in front of the camera to achieve a spatial resolution of 1.6 μm/pixel. The field of view was 4.2 mm × 3 mm. The distance between the gel sample and the camera was fixed at 20 cm, at which the phase contrast was significantly enhanced. 3D morphological structures of the test samples were numerically reconstructed from consecutively recorded projection images by using the Octopus software (inCT). For rapid data processing, the X-ray image sizes were reduced from 2560×2160 pixels to 1280×1080 pixels by 2× binning. Erroneous spots in the images were filtered out by employing dark- and flat-field imaging techniques. Sinograms were created by using normalized images for image reconstruction. The reconstructed images were analyzed and rendered with the Amira® software (Visualization Sciences Group).

Figures 4(a)–4(e) show optical and tomographic images of the fabricated agarose gel models. Figure 4(a) represents the control model type 4, and Figs. 4(b)–4(d) show the model types 1–3, respectively. The flipped structures of the model types 1, 2, and 3 are types 5, 6, and 7, respectively. Specifications of the model types 1–7 are summarized in Table I. The physical dimensions of the fabricated agarose models are 20 mm in width, 5 mm in thickness, and 15 mm in height. Figure 4(a_1-d_1) shows the optical images of the gel models, wherein isomalt particles have not been leached out yet. The second line shows 3D tomography images of porous agarose gel models after the isomalt particles are leached out (Fig. 4(a_2-d_2)). The third line presents cross-sectional images of each tomography image (Fig. 4(a_3-d_3)). As the isomalt particles are leached out, microscale pores of 750 μm in average diameter remain (a_2–d_2, a_3–d_3).
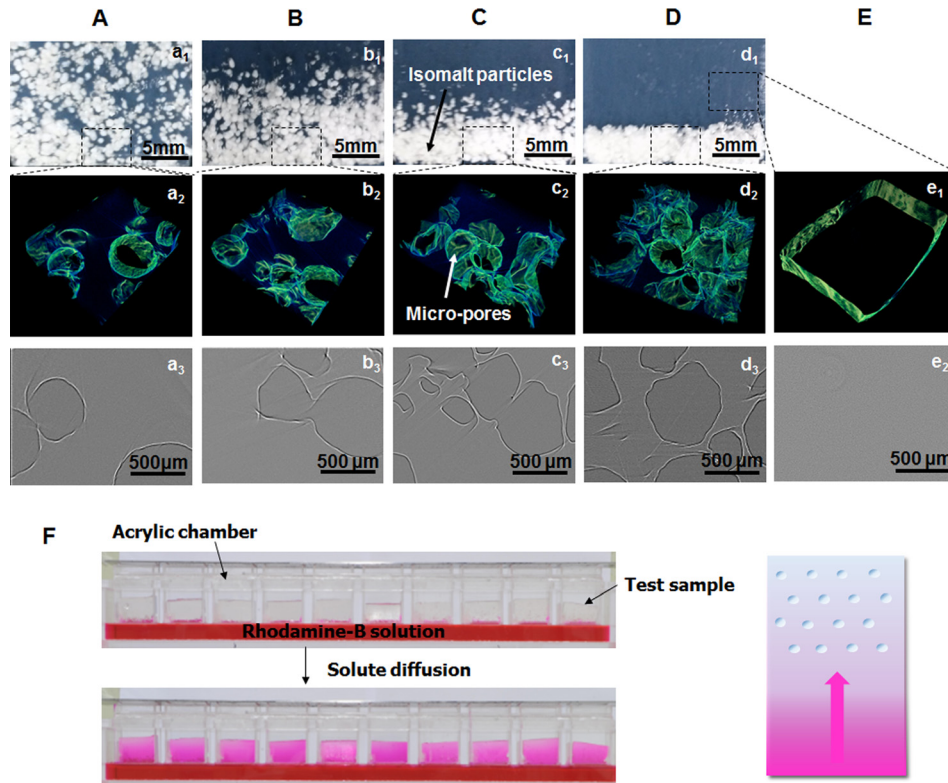
FIG. 4. (a)–(e) Optical and tomographic images of the fabricated double-layered porous agarose gel models. The first line shows the optical images of the gel models, wherein isomalt particles have not been leached out yet. The second line shows 3D tomography images of porous agarose gel models after the isomalt particles are leached out. The third line presents cross-sectional images of each tomography image. As the isomalt particles are leached out, microscale pores of $750\,\mu m$ in average diameter remain. (a_2–d_2, a_3–d_3). The agarose gel models have nanoscale pores that are invisible in X-ray images (e_1,e_2). (f) Experimental apparatus used to visualize the solution transport through the hydrogel models. Test samples were affixed in acrylic chambers, and only the bottom surface of the hydrogel models was exposed to the reservoir of Rhodamine-B solution. Evaporation was inhibited by covering all openings. The diffusion pattern of Rhodamine-B passing through the gel models was recorded with a digital camera.

The upper layer of agarose gel models has nanoscale pores that are invisible in X-ray images (e_1,e_2).[12] The average distance ($\pm$ standard error) between pores in the porous hydrogel models Figs. 4(a), 4(b), 4(c), and 4(d) is $1436\,(\pm76)\,\mu m$, $1243\,(\pm107)\,\mu m$, $1028\,(\pm55)\,\mu m$, and $796\,(\pm31)\,\mu m$, respectively. Since the average distance of each porous layer has a small standard error, the hydrogel models were modeled to have homogeneous structure. The effective diffusion coefficients of each porous layer were evaluated by using the relation of

$$D_e = \left(\frac{1}{\tau}\right)^2 \cdot D_0, \tag{2}$$

TABLE I. Summary of the structural information of seven hydrogel models.

Type #	Forward			Homogeneous	Backward		
	1	2	3	4	5	6	7
α	0.5	1	2	*	2	1	0.5
$\varepsilon_2(\%)$		0			37	50	75
$\varepsilon_1(\%)$	37	50	75			0	
E				25%			

where D_e is the effective diffusion coefficient, D_0 is the diffusion coefficient in the free path, and τ is the tortuosity factor, which can be expressed as

$$\tau = \frac{1}{2}\left[1 + \frac{1}{2}\sqrt{\emptyset} + \sqrt{\emptyset} \cdot \frac{\sqrt{\left(\frac{1}{\sqrt{\emptyset}} - 1\right)^2 + \frac{1}{4}}}{1 - \sqrt{\emptyset}}\right], \tag{3}$$

where $\emptyset$ is the void fraction ($0 \leq \emptyset = \varepsilon/100 \leq 1$) of the porous media model.[26] By using Eqs. (2) and (3), the relation between the effective diffusion coefficients and the void fraction of the material can be approximated as

$$D_e \sim D_o \cdot (-\emptyset + 1), \tag{4}$$

following a trend line with R-factor of 0.99. By using Eqs. (2)–(4), the effective diffusion coefficients of porous hydrogel models with porosity of 25%, 37%, 50%, and 75% are estimated to be $0.71\,D_0$, $0.6\,D_0$, $0.47\,D_0$, and $0.17\,D_0$, respectively.

D. Experimental method

The test samples, which were initially fully wet with deionized water, were affixed in acrylic chambers, whose bottom surfaces were opened (Fig. 4(f)). Therefore, only the bottom surfaces of the hydrogel models were exposed to the solution reservoir. Rhodamine-B solution was diluted in DI water to obtain a concentration of 50 mg/l and poured in the reservoir. Then, only the bottom surfaces of the test models were in contact with the solution. Since evaporation was inhibited by covering all openings, the solution was diffused upward by chemical potential gradient along the vertical direction. The diffusion pattern of the Rhodamine-B solution through the gel models were recorded with a digital still camera (DSD-D700, SONY) every 10 min. The exposure time was 1 sec. The images were analyzed by using the freeware ImageJ. The first image was subtracted from the destination images to remove the background effect. Light intensities from diffused Rhodamine-B solution through the test samples were measured along the vertical direction and then normalized.

E. Model: Numerical simulations

We used finite element method implemented in COMSOL Multiphysics. The existing species transport in porous media model was applied in the particular geometry of our system.

Diffusion coefficient of rhodamine-B passing through a 2% agarose hydrogel was estimated as 6×10^{-10} (m^2/s), which exhibits the best fitting between the experimental results and numerical simulation. The porosity and corresponding tortuosity factor of each layer were estimated based on Eq. (4). The reference concentration value of the solution, $c_s/c_s(L = 0) = 1$, was applied at the bottom, while the initial normalized concentration is assumed as $c_0/c_s = 0$ for the geometry handled in this study. The concentration distributions of the solution were evaluated along the vertical direction. The arriving time and the concentration at the top, when diffusion process was maintained for 2500 min, were evaluated and the results for each test sample were compared.

F. Model: Analytical approximations

The analytic modeling was started from the following double-layered diffusion equations for different concentrations of $c_i (i = 1, 2)$:

$$\frac{\partial c_1}{\partial t} = D_1 \frac{\partial^2 c_1}{\partial z^2}, \quad -L_1 < z < 0, \quad \frac{\partial c_2}{\partial t} = D_2 \frac{\partial^2 c_2}{\partial z^2}, \quad 0 < z < L_2, \tag{5}$$

where D_i is the diffusion coefficient of the corresponding layer, together with the boundary condition

$$c_{1|z=-L_1} = 1, \frac{\partial c_2}{\partial z}_{|z=L_2} = 0, \tag{6}$$

at the regions of the porous media, which are in contact with the solution reservoir and the air, respectively. The following continuity condition was imposed at the interface, where two layers meet:

$$c_{1|z=0} = c_{2|z=0}, D_1 \frac{\partial c_1}{\partial z}_{|z=0} = D_2 \frac{\partial c_2}{\partial z}_{|z=0}, \tag{7}$$

and the initial condition was

$$c_{i|t=0} = 0 \, (i = 1, 2). \tag{8}$$

After solving the problem with separation of variable method about t and z, the concentration at the top can be obtained as

$$c_2(L_2, t) = 1 - 2\sqrt{\delta} \sum_m \frac{\sec \gamma_m \operatorname{cosec}\left(\frac{\alpha \gamma_m}{\sqrt{\delta}}\right)}{\gamma_m \left(\delta + \alpha + (1+\alpha)\delta \tan^2 \gamma_m\right)} e^{-\frac{\gamma_m^2 D_1 t}{L_1^2}}, \tag{9}$$

where $\alpha = \frac{L_2}{L_1}$ and $\delta = \frac{D_2}{D_1}$ by definition. γ_m can be numerically estimated by solving $\tan \gamma_m = \frac{1}{\sqrt{\delta}} \cot(\frac{\alpha \gamma_m}{\sqrt{\delta}})$. For simplification, when time t is large enough (> 150 min), Eq. (9) can be approximated to the first term of the series as

$$c_2(L_2, t) = 1 - 2\sqrt{\delta} \frac{\sec \gamma_1 \operatorname{cosec}\left(\frac{\alpha \gamma_1}{\sqrt{\delta}}\right)}{\gamma_1 \left(\delta + \alpha + (1+\alpha)\delta \tan^2 \gamma_1\right)} e^{-\frac{\gamma_1^2 D_1 t}{L_1^2}} \tag{10}$$

with small error less than 10^{-5}.

Meanwhile, Eq. (4) leads us to rewrite the parameter δ as $\frac{-0.01\epsilon_2+1}{-0.01\epsilon_1+1}$. For $\epsilon_1 = 0$, Eq. (1) leads to the relation between α and ϵ_2 as $\epsilon_2 = (1 + \frac{1}{\alpha})E$. Then, the diffusion coefficient ratio is approximated as $\delta = -0.01(1 + \frac{1}{\alpha})E + 1$. For $\epsilon_2 = 0$, the relations of $\epsilon_1 = (1 + \alpha)E$ and $\delta = -0.01(1 + \alpha)E + 1$ are established in a similar manner. That is, δ can be considered as a function of α for a fixed porosity (E). Therefore, the solution concentration at the top surface is also a function of α. More details are provided in the supplementary material (Ref. 29).

III. RESULTS AND DISCUSSION

A. Mass diffusion through double-layered porous media

The Rhodamine-B solution was diffused from the bottom to the top of the test samples and the relative concentration distributions were compared along the vertical direction after 500 min of diffusion in Fig. 5. The indicated results were average measurement values of 6–10 test samples. The hydrogel samples were initially fully wet with deionized water and evaporation was inhibited during experiments. Therefore, the capillary effects by hydrophobic hydrogel would be ignored, and the solution diffusion occurred almost solely by chemical potential gradient along the test materials. The relative concentrations of the solution have the highest values at the bottom, since the bottom surfaces directly contacts the solution whose relative concentration is considered to be 1. Since a solution diffused along the vertical direction from the bottom to the top of the samples, the relative concentration decreases according to the height.

In Fig. 5(a), the homogeneous type 4 has higher relative concentration, compared to the three double-layered models. This can be explained intuitively by different diffusion coefficients.
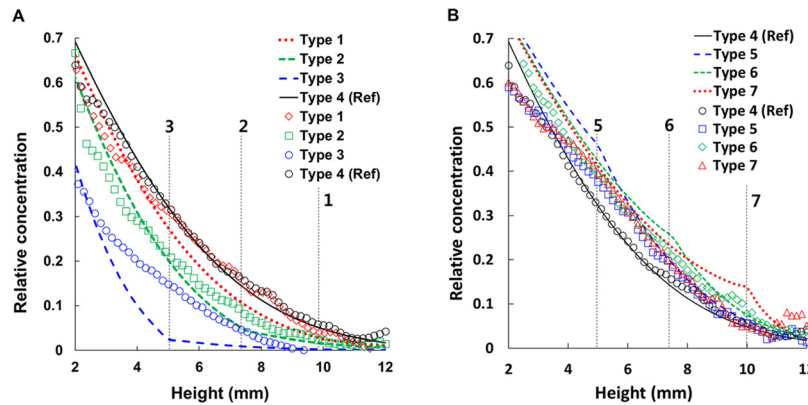
FIG. 5. Diffusion tendency of solution through double-layered porous structures in forward structure (a) and backward structure (b). The lines and dots represent the simulation and experimental results, respectively. Vertical dotted line indicates the position of the interface between the first and second layers of each model.

According to Eqs. (1) and (2), the effective diffusivities (D_e) at the first layers of the model types 1 to 4 are $0.6 \cdot D_0$, $0.47 \cdot D_0$, $0.17 \cdot D_0$, and $0.7 \cdot D_0$, respectively. The order of relative concentrations from the highest is the types 1, 2, and 3. The same order is maintained for D_e at the first layers of the models.

Related with backward structure, as shown in Figure 5(b), the three double-layered models, types 5 to 7, have higher relative concentrations than the homogeneous type 4 model. The D_e of the first layers of the model types 4 to 7 are $0.71 \cdot D_0$, $1 \cdot D_0$, $1 \cdot D_0$, and $1 \cdot D_0$, respectively. Since the D_e in the first layers of the models 5 to 7 have the same value, those three models exhibit very similar concentration distribution in the first layer. In addition, they have higher D_e values than the homogeneous type 4. When they arrive at the second layer, their relative concentrations are decreased, depending on the D_e of the second layers. The D_e at the second layers of the model types 5 to 7 are $0.6 \cdot D_0$, $0.47 \cdot D_0$, and $0.17 \cdot D_0$, respectively. The different D_e values in the first and second layers give rise to biphasic distributions of relative concentration at the interface of two layers. The general trend of the experimental data is well agreed with that of the simulation results with a correlation factor larger than 0.97. Exceptionally, the biphasic distributions at the interface where the porosity is abruptly changed are relatively insignificant in the experimental results. This distribution may result from different model structures used in simulation and experiment. Although homogeneous model structure is applied in numerical simulation, the fabricated hydrogel models do not have perfect homogeneous structure due to experimental limitations. In addition, the shape of the hydrogel matrices may be changed due to swelling during experimental procedure.[27,28]

To examine the structural effect of double-layered porous media on mass transport, numerical simulation, and theoretical analysis were conducted for the double-layered porous structures with varying thickness ratios and porosities. Figure 6 shows comparisons of the relative concentrations at the top of the structures according to the different thickness ratios of double layers after 2500 min of diffusion. The numerical values of relative concentrations are derived by applying the structural information of the models to Eq. (9). Figure 6(a) shows the variations of relative concentration of the forward structure. At a fixed porosity, as the thickness ratio α decreases, the relative concentration is increased at the top of the structures. When α is fixed, the relative concentration at the top is increased as porosity decreases. Comparing the results of $\alpha = 0.5$ to those of $\alpha = 2$, the relative concentrations are higher by 0.01, 0.32, 0.65, and 0.85 times at the porosities of E = 15%, 20%, 25%, and 30%, respectively. Here, the homogeneous structure ($\alpha = 0$) is assumed to show the highest relative concentration, irrespective of porosity. Figure 6(b) represents the results of the backward structure. At a fixed α, as porosity decreases, the relative concentrations at the top are increased. In most cases, as the α increases, more solutions are accumulated at the top of the structure. When the porosity is less than 20%, the relative concentration is not so sensitive to the variation of α. They become saturated when α is
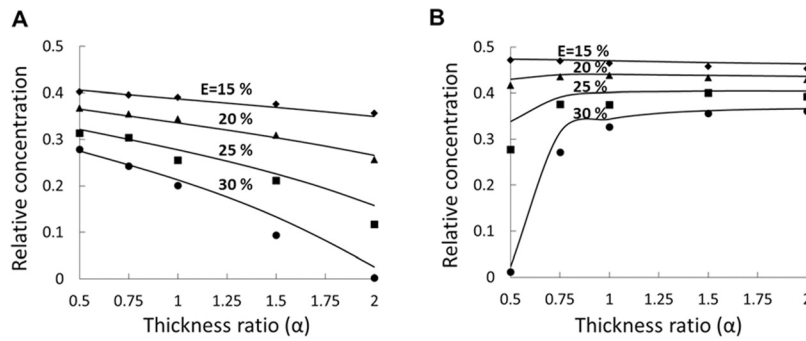
FIG. 6. Comparisons of the results of numerical simulation and theoretical analysis for the solution diffusion through the double-layered porous forward structure (a) and backward structure (b) with varying porosity and thickness ratio. The filled dots and solid lines indicate the simulation results and the analytical solution of relative concentrations at the top of the structures after 2500 min of diffusion, respectively.

larger than 1. In addition, the homogeneous structure ($\alpha = \infty$) exhibits the highest relative concentration for all porosities tested in this study.

Figure 7 shows comparisons of the solution arrival time, when the relative concentration at the top of the model geometry is greater than 0, according to the different thickness ratios of double layers. Figure 7(a) shows the variations of arrival time of the forward structure. At a fixed porosity, as the thickness ratio α decreases, the arrival time decreases. When α is fixed, as the porosity E decreases, the arrival time is decreased. Comparing the results of $\alpha = 0.5$ to those of $\alpha = 2$, the arrival times are faster by 1.06, 1.26, 2, and 2.24 times at the porosities of E = 15%, 20%, 25%, and 30%, respectively. Here, the homogeneous structure ($\alpha = 0$) shows the fastest arrival time, irrespective of porosity. Figure 7(b) represents the results of the backward structure. At a fixed α, as porosity decreases, the arrival time is decreased. In most cases, the backward structure with larger α transfer the solution faster. Based on the simulation results, the arriving time of the solution for $\alpha = 2$ is faster by 1.06, 1.26, 2.05, and 2.43 times of those for $\alpha = 0.5$ at porosities of E = 15%, 20%, 25%, and 30%, respectively. When the porosity is less than 20%, arrival time is not so sensitive to the variation of thickness ratio α. In addition, the homogeneous structure ($\alpha = \infty$) exhibits the fastest arrival time for all porosities tested in this study.

The results show that the mass transport in those models is highly influenced by porosity and the thickness ratio of the two layers. For the faster arrival time and more accumulation of solution at the top of the structure, the model with smaller porosity at fixed α is better for fast mass transport. In viewpoint of α, the relative concentration is a function of α at a fixed porosity according to Eq. (9). The double-layered models, in which pores are widely dispersed
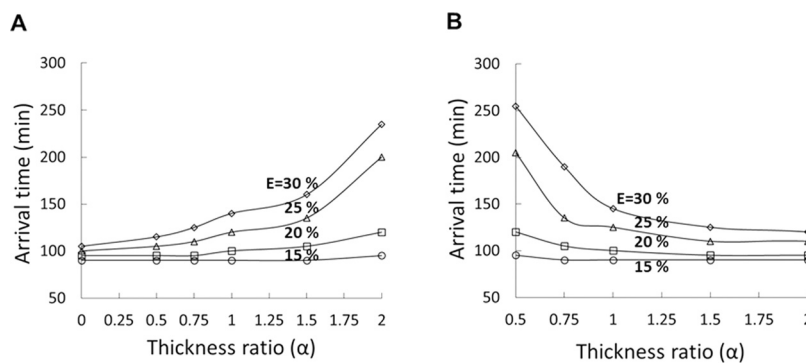

FIG. 7. Comparisons of the results of numerical simulation for the solution diffusion through the double-layered porous forward structure (a) and backward structure (b) with varying porosity and thickness ratio. The empty dots and dashed lines represent the arrival times of the solution to the top of the structures and their extension lines, respectively.
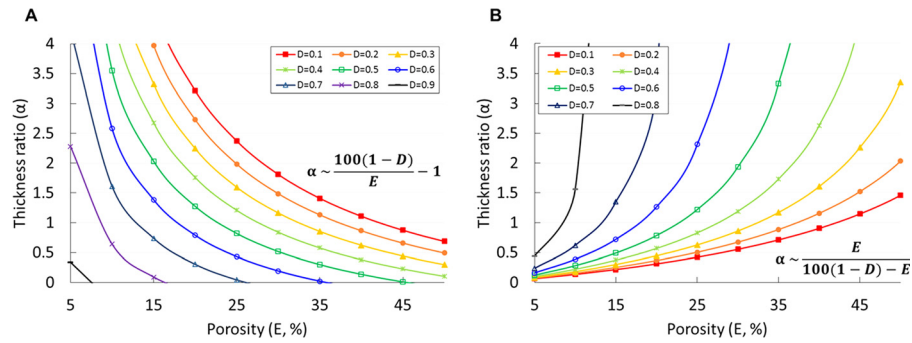
FIG. 8. Relation of α and E of the double-layered porous forward structure (a) and backward structure (b) for different D values.

throughout the structure at a fixed porosity, that is, close to the homogeneously porous structure, have advantages for fast mass transport. Especially, in case of backward structure, there was saturation range where the mass transport ability is not sensitive to the variation of thickness ratio α.

B. Structural relations

The previous results show the individual effect of α and E on mass transport with fixing one factor. However, because α and E are dependent variables, the mass transport through porous media is influenced by the two factors complementarily. Therefore, the relations between the two factors of α and E were verified by using simple a parametric study.

For the forward structure ($\varepsilon_2 = 0$), by dividing Eq. (1) with L_1 and rearranging the equation, we can obtain the relation of $\alpha = \varepsilon_1/E - 1$. Using the definition of diffusion factor $D = D_e/D_o$ and substituting $\varepsilon/100$ to $\emptyset$ in Eq. (4), the relation of $\varepsilon \sim 100 - 100D$ is obtained. By using their relations, we can obtain the following relation finally: $\alpha \sim (100 - 100D)/E - 1$. However, for the backward structure ($\varepsilon_1 = 0$), by dividing Eq. (1) with L_2 and rearranging the equation, the relation of $1/\alpha = \varepsilon_2/E - 1$ is obtained. By using the relations obtained previously, the final relation of $\alpha \sim E/(100 - 100D - E)$ is obtained. The structural relations found by parametric study between E and α for the two different double-layered porous structures are depicted in Fig. 8 for different values of D. The structural conditions along a certain line are expected to satisfy the corresponding diffusion factor D. These results can be used to provide database of basic design framework for diffusion-based mass transport through the double-layered porous structures.

IV. CONCLUSION

Inspired by plant leaves, double-layered porous hydrogel models with different thickness ratios between porous layer and nonporous layer were fabricated. The diffusion characteristics of solution in seven different hydrogel models were compared and parameter study was conducted through numerical simulation and theoretical analysis with varying structural parameters. Additionally, structural relationships required for assessing mass-transport efficiency were derived using parametric study. The experimental results and the established analytical model are well agreed with the simulation results. The solution transport in those hydrogel models is highly influenced by the porosity and thickness ratio of the two layers. Therefore, heterogeneous arrangement of porous media can control the mass transport effectively. In general, the hydrogel models with widely dispersed pores at a fixed porosity, i.e., close to a homogeneously porous structure, exhibit fast and massive mass transport. Moreover, there is a certain saturation range in backward structure, where the structure has sufficient transport ability with minimum porosity for a given thickness ratio. In addition, we clearly verified the relations between the thickness ratio and porosity which complementarily influence on mass transport ability to achieve a certain diffusion efficiency.

Biodiversity of leaf internal structures provides an ideal opportunity to test the functional similarity of the double-layered structure for effective mass transport. Most plant leaves, which can be classified into backward structure in our model system, are assumed to possess the thickness ratio of SM/PM (α) and porosity (E) for maximizing the water transport efficiency with minimum porous region (see supplementary material, Fig. S1 (Ref. 29)). This strategy might be effective for restraining excessive water lose by reducing pores.

This study is the initial basic experimental and theoretical exploration of the effective diffusion through heterogeneous porous hydrogel caused by chemical potential gradient in solution. The present analysis based on the underlying mechanism of mass transport provides the database required for determining the fundamental design parameters for practical applications such as drug delivery through porous media or hydrogel embedded microfluidic devices. Moreover, the proposed robust framework can be extended to more complex systems with different constraints, and it would be used to explore unveiled mechanisms of porous media in nature.

ACKNOWLEDGMENTS

[1]A. S. Hoffman, Adv. Drug Delivery Rev. **64**, 18 (2012).
[2]K. Khanafer and K. Vafai, Heat Mass Transfer **42**, 939 (2006).
[3]E. Kissa, J. Colloid Interface Sci. **83**, 265 (1981).
[4]I. Pezron, G. Bourgain, and D. Quere, J. Colloid Interface Sci. **173**, 319 (1995).
[5]E. Coskuntuna, A. J. Fowler, and S. B. Warner, Text. Res. J. **77**, 256 (2007).
[6]M. S. Khil, D. I. Cha, H. Y. Kim, I. S. Kim, and N. Bhattarai, J. Biomed. Mater. Res., Part B **67B**, 675 (2003).
[7]R. Jayakumar, M. Prabaharan, P. Sudheesh Kumar, S. Nair, and H. Tamura, Biotechnol. Adv. **29**, 322 (2011).
[8]F. L. Mi, S. S. Shyu, Y. B. Wu, S. T. Lee, J. Y. Shyong, and R. N. Huang, Biomaterials **22**, 165 (2001).
[9]E. W. Washburn, Phys. Rev. **17**, 273 (1921).
[10]D. Shou, L. Ye, J. Fan, and K. Fu, Langmuir **30**, 149 (2014).
[11]D. Shou, L. Ye, J. Fan, K. Fu, M. Mei, H. Wang, and Q. Chen, Langmuir **30**, 5448 (2014).
[12]K. Bal, J. Fan, M. Sarkar, and L. Ye, Int. J. Heat Mass Transfer **54**, 3096 (2011).
[13]M. Reyssat, L. Sangne, E. Van Nierop, and H. Stone, EPL (Europhys. Lett.) **86**, 56002 (2009).
[14]A. D. Gat, A. Vahdani, H. Navaz, A. Nowakowski, and M. Gharib, Appl. Phys. Lett. **103**, 134104 (2013).
[15]Y. D. Shikhmurzaev and J. E. Sprittles, Phys. Rev. E **86**, 016306 (2012).
[16]C. Liu and W. P. Ball, Adv. Water Resour. **21**, 297 (1998).
[17]Y. C. Li and P. J. Cleall, J. Geotech. Geoenviron. Eng. **136**, 1542 (2010).
[18]G. Pontrelli and F. De Monte, Int. J. Heat Mass Transfer **50**, 3658 (2007).
[19]M. Fujita, Y. Fujita, Y. Noutoshi, F. Takahashi, Y. Narusaka, K. Yamaguchi-Shinozaki, and K. Shinozaki, Curr. Opin. Plant Biol. **9**, 436 (2006).
[20]J. M. Li, C. Liu, K. P. Zhang, X. Ke, Z. Xu, C. Y. Li, and L. D. Wang, Microfluid. Nanofluid. **11**, 717 (2011).
[21]T. D. Wheeler and A. D. Stroock, Nature **455**, 208 (2008).
[22]N. Goedecke, J. Eijkel, and A. Manz, Lab Chip **2**, 219 (2002).
[23]S. J. Lee, H. Kim, and S. Ahn, "Water transport in porous hydrogel structures analogous to leaf mesophyll cells," Microfluid. Nanofluid. (published online).
[24]J. M. Li, C. Liu, Z. Xu, K. P. Zhang, X. Ke, and L. D. Wang, PloS One **7**, e50320 (2012).
[25]M. R. Slaton and W. K. Smith, Int. J. Plant Sci. **163**, 937 (2002).
[26]B. M. Yu and J. H. Li, Chin. Phys. Lett. **21**, 1569 (2004).
[27]G. Lamberti, I. Galdi, and A. A. Barba, Int. J. Pharm. **407**, 78 (2011).
[28]J. Siepmann, H. Kranz, R. Bodmeier, and N. Peppas, Pharm. Res. **16**, 1748 (1999).
[29]See supplementary material at http://dx.doi.org/10.1063/1.4914383 for analytical approximations of model systems and structural relations of real plants.